Understanding ionizing energy losses after charged particle and neutron impact in semiconductors with hybrid pixel detectors

Benedikt Bergmann
Instiute of Experimental and Applied Physics,
Czech Technical University in Prague
Prague, Czech Republic
benedikt.bergmann@utef.cvut.cz

2022 International Conference on Applied Electronics (AE) | 978-1-6654-9482-3/22/$31.00 ©2022 IEEE | DOI: 10.1109/AE54730.2022.9920076

***Abstract*—Hybrid pixel detectors of Timepix3 technology allow noiseless single particle detection and identification. We exploit this capability for a comprehensive study of ionizing energy losses and their spatial distribution in silicon sensors after exposure to charged particles and neutrons. (*Abstract*)**

Keywords—neutron radiation, radiation damage, pixel detectors, non-ionizing energy losses (NIEL), ionizing energy losses (IEL), particle detectors, pixel detectors

I. Introduction

The detection of ionizing radiation has become increasingly important for fundamental science, in medicine, for material analysis, dosimetry and in several other fields. However, the fact that ionizing radiation covers a broad range of particle types and energy ranges makes the development of radiation detectors challenging [1]. Hybrid pixel detectors of Timepix technology with their single-particle detection and processing capability are an ideal multi-purpose tool since they are noiseless and can determine location, time and/or energy of particles with high precision. The major strength of Timepix detectors is that ionizing particle interactions in the sensors are seen as imprints in the pixel matrix (tracks) with a rich set of features which can be exploited for the identification of impinging particles [2] as well as particle trajectory or reaction kinematics reconstruction. While such detectors are used in various fields of research [3], their advantages become particularly pronounced in experiments where size, weight or power consumption requirements have to be met, e.g. in Space, where they are used for the measurement of the fluxes and the directions of trapped particles in the Van-Allen radiation belts [4][5].
In the present contribution, we discuss and interpret signatures of different particles and interaction types in silicon sensors. Hereby, we put particular emphasis on the spatial distribution of the ionizing energy losses.

II. Measurement Setup

Timepix3 [6] detectors with different sensor layers were employed at accelerator facilities such as the Danish Center for Particle Therapy[1], the Super-Proton-Synchrotron (SPS) at CERN [7], and, for a Time-of-Flight measurement, at the 20 m long Flight Path 30L (FP 30L, ICE House I) of the Los Alamos Neutron Science Center (LANSCE) [8].

A. Timepix3 pixel detector

Timepix3 is a hybrid pixel detector of the Medipix/Timepix family. It consists of an ASIC based on 130 nm CMOS technology and implements 65,536 spectroscopic channels forming a 256 × 256 pixel matrix with a pixel pitch of 55 µm (total sensor area: ~1.98 cm^2) coupled to different sensor materials by means of flip-chip bump bonding. Currently available and tested sensor materials are silicon, CdTe, CZT and high resistivity chromium compensated GaAs:Cr with thicknesses ranging from 100 µm to 2 mm.
Timepix3 measures energy (ToT) and the time of arrival (ToA, resolution: 1.6 ns) simultaneously in each pixel, up to pixel hit rates of up to 40 MHits cm^{-2} s^{-1}. Detector readout is done with the Katherine Readout [9].

B. Signal creation and ionizing particle signatures

Ionizing radiation interacting in the fully depleted sensor creates free charge carriers which drift toward the corresponding electrodes, inducing a measurable current in the pixels closest to their location. In the used n-type silicon sensors, holes drift towards the pixel site and electrons towards the common backside contact. The induced currents are amplified and converted voltage signals. These are then compared to a globally adjustable threshold level (THL), which was set at 2.7 keV. The ionizing energy lost by a particle is then determined by the time the voltage pulse stays above the preset THL A continuously running clock of 40 MHz samples the voltage pulse to determine the deposited energy, by its time over threshold (ToT), and the time of arrival (ToA) with respect to the beginning of the measurement. Once the voltage crosses the discriminator threshold level (THL), the so-called Time-over-Threshold (ToT). ToT sampling is done with a 40 MHz clock. The Time-of-Arrival (ToA) is assigned to the moment of THL crossing on the upwards slope of the pulse. The accuracy of the time measurement was increased by using a 640 MHz clock from a local ring oscillator measuring the time of the actual crossing until the next rising edge of the 40 MHz base clock. The so-called time-walk, which is the dependency of the time measurement on pulse height occurs predominantly at signals with energies below ~10 keV and can be corrected for as described e.g. in [11].

C. Los Alamos Neutron Science Center (LANSCE)

At LANSCE, a white neutron energy spectrum beam (E_n up to ~600 MeV) is produced by bombarding a cylindrical tungsten target with 800 MeV protons. In spallation reaction around 10-20 neutrons are produced per impinging neutron. The proton beam is divided into 625 µs long *macropulses* with a repetition rate of 1 kHz, each containing ~348

[1] https://www.en.auh.dk/departments/the-danish-centre-for-particle-therapy/

978-1-6654-9482-3/22/$31.00 ©2022 IEEE

C. Los Alamos Neutron Science Center (LANSCE)

At LANSCE, a white neutron energy spectrum beam (E_n up

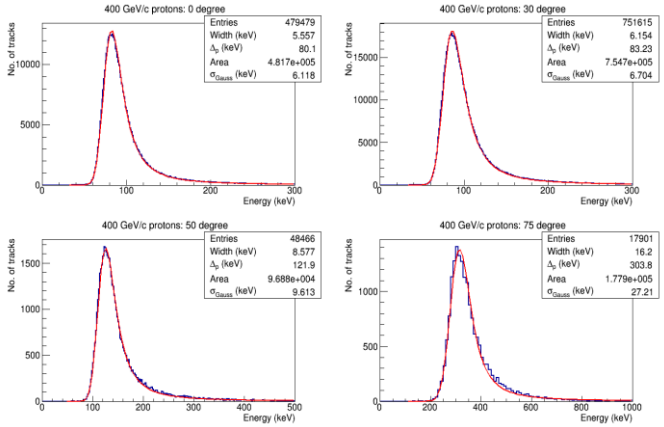

Figure 2: Ionizing energy losses of a 500 GeV/c proton hitting a 300 µm thick silicon sensor at different angles. The energy deposition is described by a Landau function convolved with a Gaussian. The fits are indicated.

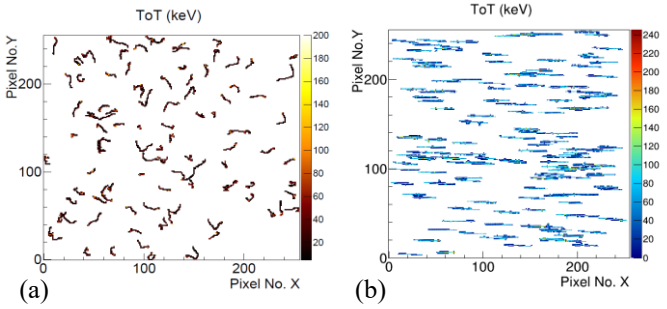

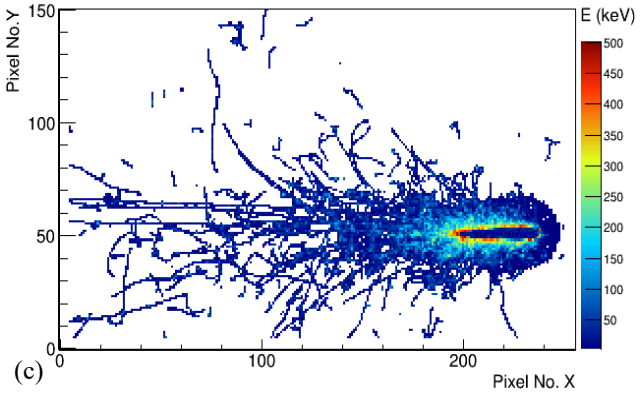

Figure 1: Signatures of different particles interacting in silicon: (a) 800 keV electrons (from [1]); (b) 160 MeV protons and (c) 120 GeV/c lead ion (from [13]); In (b) and (c) the particle impact was at an angle of 70 degrees with respect to the sensor normal.

to ~600 MeV) is produced by bombarding a cylindrical tungsten target with 800 MeV protons. In spallation reaction around 10-20 neutrons are produced per impinging neutron. The proton beam is divided into 625 µs long *macropulses* with a repetition rate of 1 kHz, each containing ~348 *micropulses* separated at 1.8 µm. Reference neutron fluences were provided by a calibrated Uranium fission chamber [10].

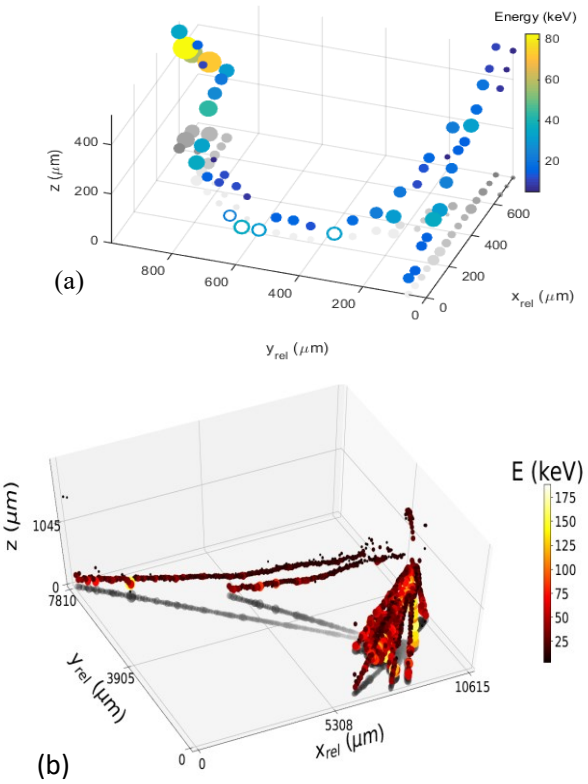

Figure 3: 3D reconstruction of: (a) a 120 GeV/c pion track measured at SPS in a 500 µm thick silicon sensor; (b) a spallation reaction in a 2 mm thick CdTe sensor placed in a 40 GeV/c pion beam. The projection in the xy-plane depicts the z-coordinate in gray scale. The radius of the points scales linearly with energy deposition. From [11][12].

III. Ionizing Particle Signatures

Ionization density and secondary particle creation depend on the impinging particle's type, momentum and nuclear charge. Different particle species and interaction types can be identified using characteristic footprints. Examples are shown in *Figure 1*.

The most probable ionizing energy loss for a particle of given energy and type can be calculated by the Bethe-Bloch formula assuming Coulomb interaction of the charged projectile with the electrons in the sensor. The dispersion around the mean value is given by a Landau-Vavilov distribution. In the spectra shown in *Figure 2* the limited energy resolution of the detectors results in a Gaussian smearing of the Landau curves.

The precise time tagging feature combined with the small pixel effect in the sensor make it possible reconstruct the trajectory of particles within a sensor in 3 dimensions (voxel size of ~50 µm x 50 µm x 50 µm), forming a semiconductor Time Projection Chamber [11][12][13]. This provides

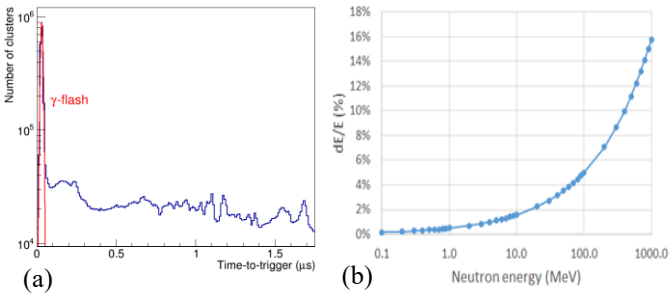

Figure 4: (a) Measured number of clusters as a function of the time to the received trigger signal; (b) Calculated neutron kinetic energy resolution as a function of incident neutron energy.

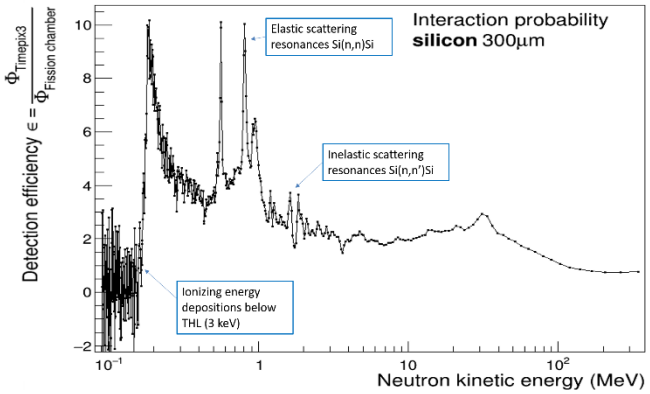

Figure 5: Fast neutron interaction probability as a function of neutron incident energy for a 300 μm thick silicon sensor. Processes leading to the discernible structures are labeled.

additional information for improved impact angle and particle type determination. Examples of 3D reconstructed tracks are shown in *Figure 3*.

IV. Neutron Interactions

A. Time-of-flight (TOF) technique

Timepix3's time resolution together with the pulse structure of the LANSCE neutron beam allow neutron energy determination using the time-of-flight (TOF) technique. Therefore, the Timepix3 time measurement is reset upon the *micropulse* trigger signal.

Figure 4(a) shows a spectrum of the particle arrival times after receiving the trigger signal. Prompt γ-rays arriving at the detector first are seen as a peak (at t_γ). We calculate the neutron TOF by their delay related to this signal as $t_{flight} = t_n - (t_\gamma - d/c)$, where t_n is the measured time after trigger, d is the distance to the target and c the speed of light. The neutron energy is given by $E_n = (\gamma - 1) \times M_n$, with $\gamma = (1 - \beta^2)^{-1/2}$ and $\beta = \frac{t_n}{t_\gamma}$. Further details on the method can be found in [14][15][16]. Since the jitter of the trigger can be neglected, neutron kinetic energy resolution purely depends on time resolution of the detector. The relative kinetic neutron energy resolution is shown as a function of the incident neutron energy in *Figure 4(b)*, conservatively assuming a time resolution of $dt \sim 8$ ns.

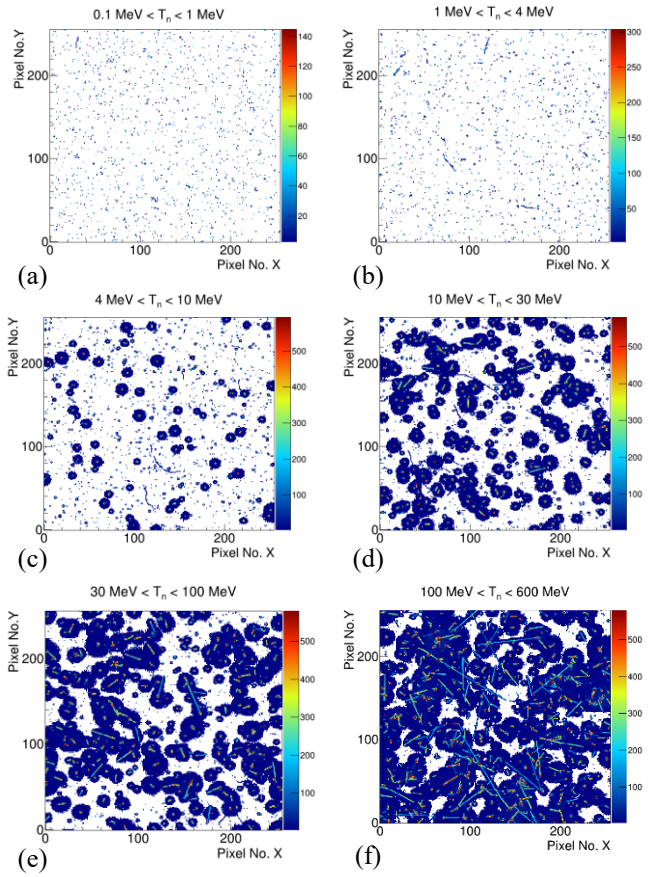

Figure 6: Signature of neutrons interacting in the silicon sensor for the energy intervals 0.1-1 MeV (a); 1-4 MeV (b); 4-10 MeV (c); 10-30 MeV (d); 30-100 MeV (e) and 100-600 MeV (f).

B. Neutron interactions

Figure 5 depicts the probability that a neutron which hits the 300 μm thick silicon sensor is registered. The probability is presented as a function of the incident neutron energy. Below ~2 MeV several peak structures are visible, which are due to resonances of elastic $^{28}Si(n,n)^{28}Si$ and inelastic $^{28}Si(n,n')^{28}Si$ scattering off the silicon atoms in the lattice. Due to the detector threshold of 3 keV neutrons are detectable if their energy is above ~200 keV [14]. The morphology of neutron interactions is shown in *Figure 6* for different neutron energy intervals. Up to 4 MeV the measureable signal is created by recoil silicon losing part of its energy by ionization. The thresholds for inducing nuclear reaction on silicon are reached at 2.75 MeV and 4 MeV for $^{28}Si(n,\alpha)^{25}Mg$ and $^{28}Si(n,p)^{28}Al$, respectively. Above 20 MeV, fragmentation reactions with several outgoing particles appear.

The ionizing energy deposition spectra of the secondary charged particles after neutron impact are shown in *Figure 7*. Scattering processes are seen as a continuous spectrum from the detector threshold up to an edge, related to neutron backscattering (*Figures 7(a)-(c)*) (see also [14]). In nuclear reactions the signatures are mainly created by the lighter reaction products (protons, α-particles, …). The peak structure in *Fig. 7(c)* is due to the structure of the daughter nuclei. At 20 MeV (*Figure 7(d)*), different processes overlap,

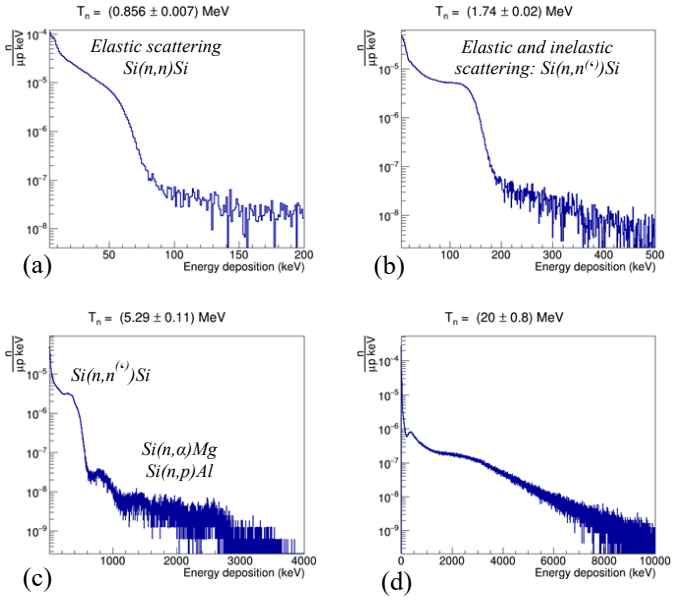

Figure 7: Ionizing energy deposition spectra after fast neutron interactions in silicon at (quasi-)monoenergetic neutron impact with energies (a) 0.856 ± 0.007 MeV; (b) 1.74 ± 0.02 MeV; (c) 5.29 ± 0.11 MeV and (d) 20.0 ± 0.8 MeV.

secondaries leave the thin sensor and high energy depositions are smeared out by electronics saturation, resulting in a continuous spectrum. The results can be compared with the simulated spectra presented in [17].

V. Conclusion

Ionizing energy depositions and their spatial distribution were presented after charged particles and neutron interactions in silicon.

Acknowledgment

The work has been done in the frame of the Medipix collaboration. This work has benefited from the use of the Los Alamos Neutron Science Center at LANL. This facility is funded by the U.S. Department of Energy under Contract No. DE-AC52-06NA25396.

References

[1] B. Bergmann, "Improved methodology of the recognition and separation of x-rays, neutrons and charged particles using hybrid active pixel detectors", PhD thesis, Erlangen Center for Astroparticle Physics, Friedrich-Alexander-University Erlangen-Nürnberg, 2019.

[2] T. Holy, E. Heijne, J. Jakubek, S. Pospisil, J. Uher and Z. Vykydal, "Pattern recognition of tracks induced by individual quanta of ionizing radiation in Medipix2 silicon detector," Nucl. Inst. Meth. A, Vol. 591, Issue 1, pp 287-290, 2008.

[3] R. Ballabriga, M. Campbell and X. Llopart, "ASIC developments for radiation imaging applications: The Medipix and Timepix family," Nucl. Inst. Meth A, Vol. 878, 2018.

[4] St. Gohl, B. Bergmann, H. Evans, P. Nieminen, A. Owens and S. Pospisil, "Study of the radiation fields in LEO with the Space Application of Timepix Radiation Monitor (SATRAM)," Advances in Space Research 63, Issue 5, pp 1646-1660, 2019.

[5] St Gohl, B. Bergmann, C. Granja, A. Owens, M. Pichotka, S. Polansky, and S. Pospisil, "Measurement of particle directions in low earth orbit with a Timepix," Jour. Instr. 11, C11023, 2016.

[6] T. Poikela, J. Plosila, T. Westerlund, M. Campbell, M. De Gaspari et al, "Timepix3: A 65 k channel hybrid pixel readout chip with simultaneous toa/tot and sparse readout," Journ. Instr. 9, C05013, 2014.

[7] N.A. Tahir, R. Schmidt, M. Brugger, R. Assmann, A.V. Shutov et al, "The CERN Super Proton Synchrotron as a tool to study high energy density physics," New J. Phys., Vol. 10, 073028, 2008.

[8] P.W. Lisowski and K.F. Schoenberg, "The Los Alamos Neutron Science Center," Nucl. Inst. Meth. A, vol 562, Issue 2, pp 910-914, 2006.

[9] P. Burian, P. Broulim, M. Jara, V. Georgiev and B. Bergmann, "Katherine: Ethernet Embedded Readout Interface for Timepix3," Jour. Instr., Vol. 12, C11001, 2017.

[10] S.A. Wender, S. Balestrini, A. Brown, R.C. Haight, C.M. Laymon, et al., "A fission ionization detector for neutron flux measurement at a spallation source," Nucl. Inst. Meth. A, vol. 336, Issues 1-2, pp 226-231, 1993.

[11] B. Bergmann, M. Pichotka, S. Pospisil, J. Vycpalek, P. Burian et al., "3D track reconctruction capability of a silicon hybrid active pixel detector," Eur. Phys. J. C 77, 421, 2019.

[12] B. Bergmann, P. Burian, P. Manek and S. Pospisil, "3D reconstruction of particle tracks in a 2 mm thick CdTe hybrid pixel detector,"Eur. Phys. J. C 79, 165, 2019.

[13] B. Bergmann et al. (MoEDAL collaboration), "Timepix3 as solid-state time-projection chamber in particle and nuclear physics," in proceedings of th 40th international Conference on High Energy Physics – PoS (ICHEP2020), vol. 390, p. 720, 2021.

[14] B. Bergmann, S. Pospisil, I. Caicedo, J. Kierstead, H. Takai and E. Fröjdh, "Ionizing Energy Depositions After Fast Neutron Interactions in Silicon", in IEEE Transactions on Nuclear Science, vol. 63, no. 4, pp. 2372-2378, Aug. 2016, doi: 10.1109/TNS.2016.2574961.

[15] B. Bergmann, R.O. Nelson, J.M. O'Donnell, S. Pospisil, J. Solc, H. Takai and Z. Vykydal, "Time-of-Flight measurement of fast neutrons with Timepix detectors," Journ. Instr., vol. 9, C05048, 2014.

[16] B. Bergmann, I. Caicedo, C. Leroy, S. Pospisil and Z. Vykydal, "ATLAS-TPX: a two-layer pixel detector setup for neutron detection and radiation field characterization," Journ. Instr., vol. 11, P10002, 2016.

[17] D. Lucsanyi, R. G. Alia, K. Bilko, M. Cecchetto, S. Fiore et al, "G4SEE: A Geant4-Based Single Evemt Effect SimulationToolkit and Its Validation Through Monoenergetic Neutron Measurements," in IEEE TNS, Vol. 69, No. 3, March 2022.